Nd^{3+} and Nb^{5+} Co-Substitution Inducing a Large Electrocaloric Response in $Na_{0.5}Bi_{0.5}TiO_3$ Lead-Free Ceramics

Kumara Raja Kandula, Tirupathi Patri, and Saket Asthana**

Nd^{3+} and Nb^{5+} co-substituted $(Na_{0.5}Bi_{0.49}Nd_{0.01})Ti_{1-x}Nb_xO_3$ lead-free ceramics are synthesized by conventional solid-state reaction method. The X-ray diffraction study revealed that NBNT-Nb-0 ($x = 0.00$) ceramics exhibit single phase monoclinic crystal with *Cc* phase while NBNT-Nb-1 ($x = 0.00$) ceramics exhibited a dual phase with *Cc* + *P4mm* coexistence of monoclinic and tetragonal systems. The temperature-dependence dielectric study revealed the existence of ferroelectric and antiferroelectric transformations in two independent regions. Further temperature-dependent strain vs. electric field measurements strengthen the ferroelectric to antiferroelectric transformation in the present ceramics. The induced electrocaloric effect (ECE) response showed that a significant change in temperature (ΔT) is obtained at 50 kV cm^{-1} fields: about 0.69 K for NBNT-Nb-0 and 0.81 K for NBNT-Nb-1 ceramics, respectively. The maximum isothermal entropy change (ΔS) is found to be 0.95 and 1.02 J kg^{-1} K^{-1} for NBNT-Nb-0 and NBNT-Nb-1 ceramics obtained at 50 kV cm^{-1}, respectively. The simultaneous presence of ECE response and isothermal change in entropy (ΔS) is an open window for great potential applications in the field of electronic devices.

1. Introduction

Over the last few decades, advanced dielectric and ferroelectric materials have been studied widely due to its large number of technological applications such as memory devices and energy storage capacitors.[1–5] In recent years, it has been observed that "electrocaloric effect" in ferroelectrics and relaxor ferroelectric materials, resembles with the well-known magnetocaloric effect (MCE).[6] Such electrocaloric effect (ECE) can be defined as the reversible temperature and entropy change an insulating polarizable material during removal of the electric field under adiabatic conditions. These reversible temperature changes serve as a refrigerant coolant by temperature controlling devices similar to magnetocaloric materials. These intriguing properties have thus created a lot of interest among researchers toward developing new electrocaloric materials owing to their practical applications such as miniaturized and high efficient cooling controlling devices.[7–9]

In 2006, Mischenko et al., reported a giant ECE ($\Delta T = 12$ K and $\Delta S = 8$ J kg K^{-1}) in $Pb(Zr_{0.95}Ti_{0.05})O_3$ (PZT) thin film of thickness about 350 nm.[10] The observed large ECE value in thin film was attributed due to their high breakdown field. Later on, several researchers explored the electrocaloric effect in Pb-based (PZT, PMN-PT, PBZ etc. . .) thin films.[8–9] Most of these studies revealed large ECE value due to their high breakdown field. It was noted that their lower heat capacity of film thickness hampered their application for large-scale solid-state cooling devices.[11–12] Additionally, the inherent toxicity of lead oxide and its high vapor pressure during sintering process caused serious problem to human health and environment. To overcome these limitations, researchers are highly motivated to develop lead free bulk ceramic materials and to successfully be able to enhance their E_C values. Among all reports, Sodium Bismuth Titanate ($Na_{0.5}Bi_{0.5}TiO_3$) was found to be one of the promising candidates to replace lead-based ECE materials. Although, ($Na_{0.5}Bi_{0.5}TiO_3$) has long range ferroelectric and several structural phase transitions from room temperature (RT) to 800 K. It has few drawbacks such as (a) large coercivity (E_C) 73 kV cm^{-1} and (b) high dielectric loss.[13–14] To overcome these above affirmations, several research groups attempted rare earth substitution in NBT at A-site. Recent reports on rare-earth (RE) based NBT materials showed enhanced electrical and dielectric properties which lead to act as a candidate in lead free ferroelectric applications.[15–18] A few studies have been reported regarding enhanced electrocaloric effect in lead-free NBT-based ceramics by substitution of different rare earth elements.[19] Zannen et al. reported that Dy–NBT showed an abnormal electrocaloric change in adiabatic temperature at ≈2 K and similar kind of results were also observed in Gd and Nd-modified NBT ceramics.[20–21] Recently, a better induced temperature change (ΔT) with large ECE behavior on Nd substituted NBT ceramics was reported elsewhere.[22] Conversely, the ECE response of the reported Nd-NBT was found to be significantly lower than that reported in the lead-based

K. R. Kandula, Dr. S. Asthana
Advanced Functional Materials Laboratory
Department of Physics
Indian Institute of Technology Hyderabad, Kandi (V)
Sangareddy, Telangana 502285, India
E-mail: asthanas@iith.ac.in

Dr. T. Patri
Department of Physics
Rajiv Gandhi University of Knowledge Technologies
(AP-IIIT) RK Valley 516330, India
E-mail: ptirupathi36@gmail.com

DOI: 10.1002/pssb.201900001

 © 2019 WILEY-VCH Verlag GmbH & Co. KGaA, Weinheim

systems.[23] Hence to, overcome this issue and to improve ECE values in Nd- substituted NBT ceramic, we modified the co-substitute NBT, that is, Nd^{3+}–Nb^{5+} substituted NBT. In this present paper, we have reported the structural and temperature dependent dielectric properties of Nb^{5+} doping on NBT-Nd ceramics. The electrical properties as well as enhanced electrocaloric response in these ceramics was also studied and reported.

2. Experimental Section

The polycrystalline ceramics of $(Na_{0.5}Bi_{0.49}Nd_{0.01})Ti_{1-x}Nb_xO_3$ ($x = 0.00$ and 0.01) (abbreviated as NBNT-Nb-0 and NBNT-Nb-1) were synthesized by using conventional solid-state reaction technique, with the help of high-purity (≥99.8%) ingredients (raw materials): Bi_2O_3, Nd_2O_3, Na_2CO_3, Nb_2O_5, and TiO_2 in the stoichiometric ratio and milled in presence of 2-Isopropanol (IPA) medium and then dried. Further, to reduce the loss of composition of Bi_2O_3 and Na_2CO_3 during high temperature sintering, an excess amount 0.3 mol% of Bi and Na were taken while primary mixing of these raw materials followed by ball milling. The fine grounded powder was then calcinated at 800 °C for 3 h. Each composition was again ball milled for 10h and further milled, sieved, and compacted into a circular disc of diameter (ø = 8 mm) and finally sintered at 1150 °C for 3 h in air medium with the heating rate of 5 °C min^{-1}. The structural phase purity of these polycrystalline powders were analyzed by XRD technique by using an (PANlytical X'pert-pro with CuK_α $\lambda = 1.5406$ Å). Temperature dependent dielectric measurements were performed on the silver coated sintered ceramics discs of thickness in between (1–1.5 mm) from 30 to 500 °C with frequency variation of 5 kHz to 1 MHz by using (Wayne Kerr 6500B) impedance analyzer. The temperature dependent polarization (P) v/s electric field (E) measurements and field induced strain measurements were carried out by using TF-Analyzer 2000 (aix ACCT systems, GmbH) on the silver-coated samples.

3. Results and Discussion

3.1. Structural Analysis

The XRD pattern of NBNT-Nb-0 and NBNT-Nb-1 ceramics within the range of $20° \leq 2\theta \leq 80°$ is displayed in **Figure 1**a, which showed a pure perovskite structure without coexistence of secondary phases. The insight view and deconvolution of particular Bragg reflection in between 39°–41°, is shown inset Figure 1b,c. NBNT-Nb-0 ceramics showed a single peak in given range (38° to 41°), which was characterized by the monoclinic structure with *Cc* space group. Further, NBNT-Nb-1 compound, exhibited a peak $(110)_m$, which splits into two Bragg reflections (003) and (021) peaks, respectively. The peak profiles were found to be located at 38°–41°, there by which enabled us to identify the possible evolution of other structural phases as is clearly demonstrated in Figure 1b,c. The (110) peak shifted toward a higher angle which indicated a lattice shrink due to the mismatch of ionic radii between Ti^{4+} (CN = 6, 0.65Å) and Nb^{5+} (CN = 6, 0.61Å), which induce the formation of A-site vacancies (Na/Bi) by substitution of Nb^{5+} in B-site. In order to know the exact phase contribution quantitatively in the ceramics, we carried out structural analysis by Rietveld refinement technique using Full-prof software.

Figure 2a,b displayed Rietveld refined X-ray diffraction pattern of NBNT-Nb-0 and NBNT-Nb-1 ceramics. The XRD patterns were refined with pattern matching different space groups such as R3c, Cc, P4mm, Pbnm, and P4bm etc. It is well known reported that RT pure NBT is as a stable rhombohedral with R3c space group.[24] Keeping this in mind, our research group refined the structure with R3c space group initially to investigate the crystal system. However the R3c model provides a rationally good quality of fit ($R_p = 11.45\%$) for NBNT-Nb-0 ceramic. The calculated pattern for (110) and (111) multiple reflections in the R3c model deviates from the observed pattern at maximum intensities. Therefore, we modeled with Cc space group, since Cc is a subgroup of the R3c space group. For NBNT-Nb-0, it is well fitted with monoclinic Cc space group as shown in Figure 2a. Satisfactory reliability factors were obtained for profile adjustment with monoclinic Cc space group, that is, $R_P = 4.04$ $R_{wp} = 3.15$ and $\chi^2 = 2.63$, provided in **Table 1**. Further for NBNT-Nb-1, we observed an evolution of extra peak identical to a tetragonal reflection of $(111)_{pc}$ after deconvolution (shown inset of Figure 1b). Nevertheless, this $(111)_{pc}$ peak was almost a negligible contribution for NBNT-Nb-0 ceramics. For NBNT-Nb-1 the contribution of P4mm space group taken under consideration and the refinement had been performed with the help of duel phase model Cc + P4mm. This model gave a satisfactory fit for NBNT-Nb-1 with Cc + P4mm, is shown in Figure 2b. The obtained reliable factors and corresponding lattice parameters values were showed in Table 1. It became clear that the additional peak in the $(111)_{pc}$ peak profile at 39°–41° is characteristic of tetragonal *P4mm* phase. Hence, it can be confirmed that Nb substitution lead to introduce the tetragonal phase in NBNT-Nb-1 ceramics, that is, Cc + P4mm.

Further, to confirm more evidently the associated phase transition in NBNT-Nb-0 and NBNT-Nb-1 ceramics, we performed room temperature current v/s electric field (I–E) characterizations. **Figure 3** demonstrated current v/s electric field (I-E) loop for both the ceramics, which showed typical ferroelectric characteristic. For NBNT-Nb-0, two peaks at $\pm E_c = 70\,kV\,cm^{-1}$ were observed which are symmetric in nature, corresponds to the coercivity of characteristic polarization loops. While for NBNT-Nb-1 ceramics (shown Figure 3 (red color)), I–E loop exhibits four distinct peaks at $\pm E_F$ ($E_F = 55.24\,kV\,cm^{-1}$) and $\pm E_1$ ($E_1 = 25.40\,kV\,cm^{-1}$). The peak at $+E_F$ represents a transition from part of antiferroelectric (AFE) phase to ferroelectric (FE) phase when the ceramics are applied by a positive electric field.[25–26] It is well reported in NBT based ceramics, the tetragonal phase shows antiferroelectric characteristics while rhombohedral and/or monoclinic phase is ferroelectric characteristics. The noticed four distinct peaks in I-E loop indicate the existence of dual phase in NBNT-Nb-1 ceramics. Henceforth, it can confirm the coexistence of both monoclinic and tetragonal (i.e., Cc + P4mm) phase in NBNT-Nb-1 ceramics which is consistent with XRD studies. In addition, the current density (J) v/s electric fields (E) of both ceramics were carried and represented inset Figure 3. From the leakage current density graph, we noticed the symmetry nature of the current density in

© 2019 WILEY-VCH Verlag GmbH & Co. KGaA, Weinheim

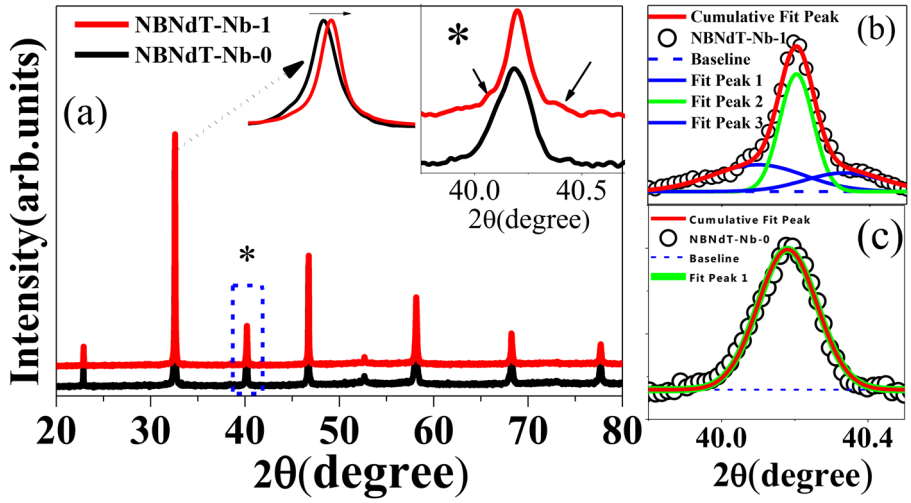

Figure 1. a) Room temperature powder X-ray diffraction patterns of NBNT-Nb-0 and NBNT-Nb-1; the main intense peak (110) peak shifting toward higher angle shown in the inset. b,c) De-convolution of $(111)_{pc}$ peak in the angle 39°–41° region.

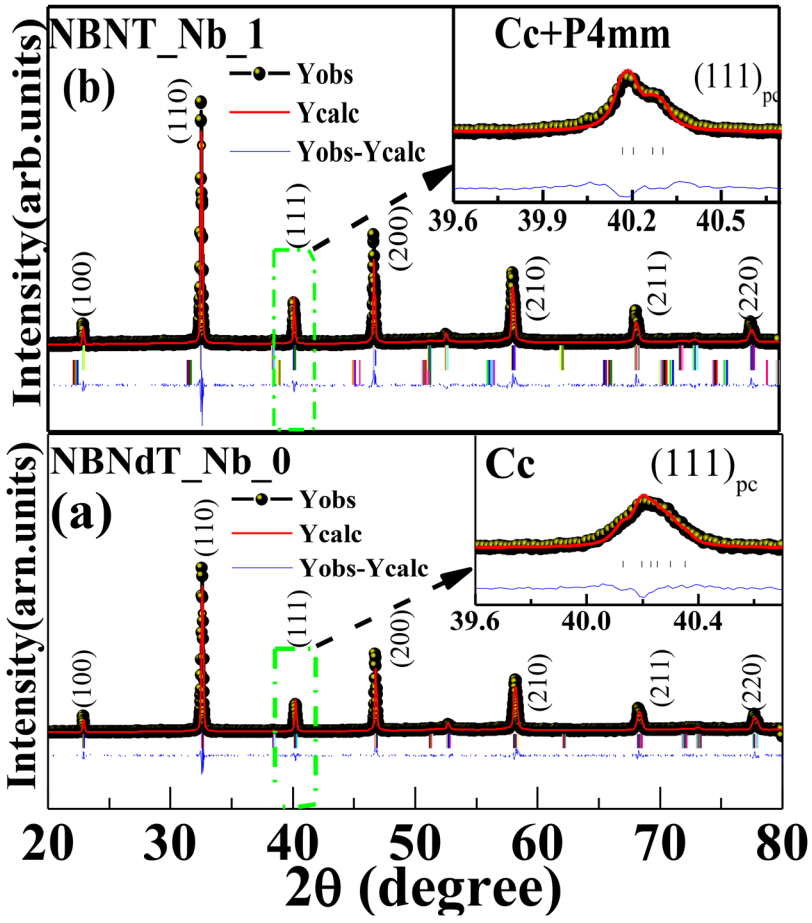

Figure 2. a,b) Rietveld refinement pattern of NBNT-Nb-0 and NBNT-Nb-1 ceramics. a) NBNT-Nb-0 with monoclinic Cc phase model. NBNT-Nb-1 with two phase monoclinic+tetragonal (Cc + P4 mm) phase. The insets highlight the enlarged view in the region 39°–41° of $(110)_{pc}$.

both positive and negative field regions about $E = 0$ kV/cm. The obtained leakage current density for NBNT-Nb-1 slightly lower compared to NBNT-Nb-0, which is lower than the pure NBT system.[27–34] The observed leakage current values reflect its improved electrical properties due to presence of rare earth substitution in NBT. The low leakage current in the order of 10^{-9} produces negligible Joule heating, which is beneficial for practical application.

3.2. Temperature Dependence Dielectric Studies

The temperature dependence dielectric constant (ε) and dielectric loss (i.e., tanδ) with a variation of temperature of both ceramics at selected frequencies between 5 kHz-1 MHz were shown in **Figure 4**a,b. Both ceramics were employed at two characteristic dielectric anomalies near around 423 K and near at 623 K, respectively.[35] The first dielectric anomaly was observed at 429 K for NBNT-Nb-0 and 423 K for NBNT-Nb-1 respectively, which is called as depolarization temperature (T_d) causing the material to undergo a phase transition ferroelectric to antiferroelectric phase. The second phase transition was observed at 623 K for NBNT-Nb-0 and at 632 K for NBNT-Nb-1, respectively. The second anomaly was observed at maximum value of dielectric constant, the corresponding temperature represented as Curie temperature (T_m). This Curie temperature (T_m) is accountable for antiferroelectric to paraelectric transitions; similar to those found in NBT based ceramics. For NBNT-Nb-1 (mixed phase) composition, it shows

© 2019 WILEY-VCH Verlag GmbH & Co. KGaA, Weinheim

Table 1. Structural refined parameters of monoclinic (Cc) along with tetragonal (P4 mm) phase for NBNT-Nb-1 ceramic.

Cc	x	y	z
Na/Bi/Nd	0.0000	0.2474	0.0000
Ti/Nb	0.2495	0.2696	0.7478
O_1	−0.0088	0.2057	0.5187
O_2	0.2254	0.5165	−0.0389
O_3	0.2642	0.0239	0.0482
Lattice parameters	$a = 9.5150\text{Å}, b = 5.4890\text{Å}, c = 5.4959\text{Å}, \alpha = \gamma = 90^\circ, \beta = 125.2810^\circ$		
P4 mm	x	y	z
Na/Bi/Nd	0.0010	0.2474	0.0000
Ti/Nb	−1.1407	0.2567	0.6856
O_1	0.5000	0.5000	0.4759
O_2	0.5000	0.0000	0.7560
Lattice parameters	$a = 4.0209\text{Å}, b = 4.0209\text{Å}, c = 3.9747\text{Å}, \alpha = \beta = \gamma = 90^\circ$		
Cc(94%)+P4mm(6%) : $R_p = 4.04$ and $R_{wp} = 3.15$, $X^2 = 2.63$			

a lower depolarization temperature while compared to NBNT-Nb-0 ceramics, which indicate the reduction of the stability of ferroelectric domains. Compared with the compositions consisting of a single phase, the coexistence of a mixed phase created a more stress that leads to the incompatibility of their crystal lattices, resulting in a decrease of the thermal stability in the long-range ferroelectric domains. On the other hand, the noted T_m shifted toward a higher temperature while Nb substitution indicated the stability of antiferroelectric domain in the long range. In addition to the shifting of dielectric phase transitions (T_d & T_m) there is a significant modification in the dielectric constant as well as dielectric loss parameters also. The variations in these transition temperatures in case of NBNT-Nb-1 can be understood by bond enthalpy concept. The structural distortion is mainly due to the strong hybridization between 4p electrons of Nb^{5+} and 2p electrons of O^{2-} as compared with the hybridization which originated from 3d lone pair electrons of Ti^{4+} and 2p electrons of O^{2-} ions. Here the bond enthalpy of the Nb-O ≅771 kJ mol^{-1} is higher compared with the Ti-O≅672 kJ mol^{-1} as shown in Figure 4a. The substitution of Nd ion in NBT matrix affected the reduction in dielectric constant (ε) ≈503 which was observed at room temperature.[36] Further, doping of Nb^{5+} in NBNT ceramics showed enhancement in dielectric constant (ε) ≈775 as well as dielectric loss at room temperature, indicated that Nb substitution in NBNT ceramics leads to an increase in conductivity.

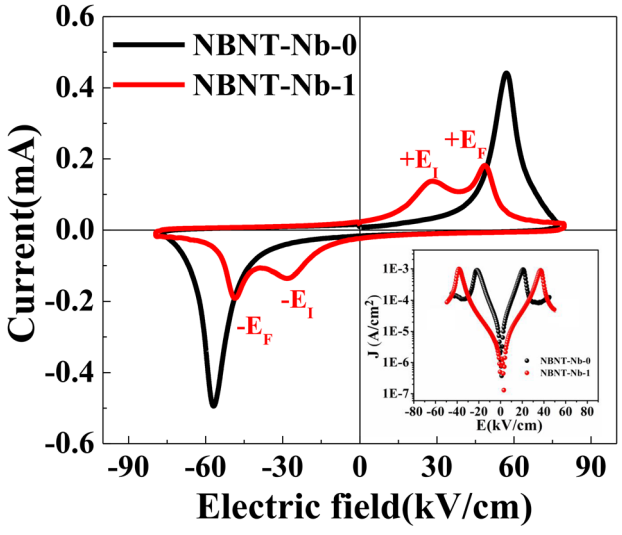

Figure 3. Room temperature current v/s electric field (*I–E*) loops of NBNT-Nb-0 and NBNT-Nb-1 both ceramics at field strength of 75 kV cm^{-1} and 1 Hz frequency.

3.3. Ferroelectric and Electrocaloric Studies

Temperature dependent *P–E* hysteresis loops and bipolar strain v/s electric field (*S–E*) curves for both the ceramics were measured under an applied electric field from 0 to 80 kV cm^{-1} within the temperature range of 313 K to 378 K at a frequency of 1 Hz, as shown in **Figure 5**a,d. NBNT-Nb-0 ceramics, showed well saturated P-E loops with pure classical ferroelectric behavior having saturation (P_s) and remnant (P_r) polarization values 33.3 μC cm^2 and 30 μC cm^{-2} respectively at 313 K. When compared to pure NBT, the noted polarization for NBNT ceramic was found to be much significant and slightly higher with those from the literature reports.[37] Although temperature dependent P-E loops up to 368 K it does not show any significant change in the shape of P-E loops, excluding a decreases in the P_r and P_s values. This behavior indicates a pure ferroelectric character of NBNT ceramics which is measured at different temperature intervals. The enhancement of ferroelectric property in NBNT-Nb-0 might be due to the incorporation of the nonvolatile Nd^{3+} in NBT control which compensate loss and reduce the number of oxygen vacancies might be created due to (Bi^{3+} and/or Na^{+1}) volatility at high temperature sintering. It is clearly shown that with increasing temperature polarization value decrease irrespective of the applied electric field, which

© 2019 WILEY-VCH Verlag GmbH & Co. KGaA, Weinheim

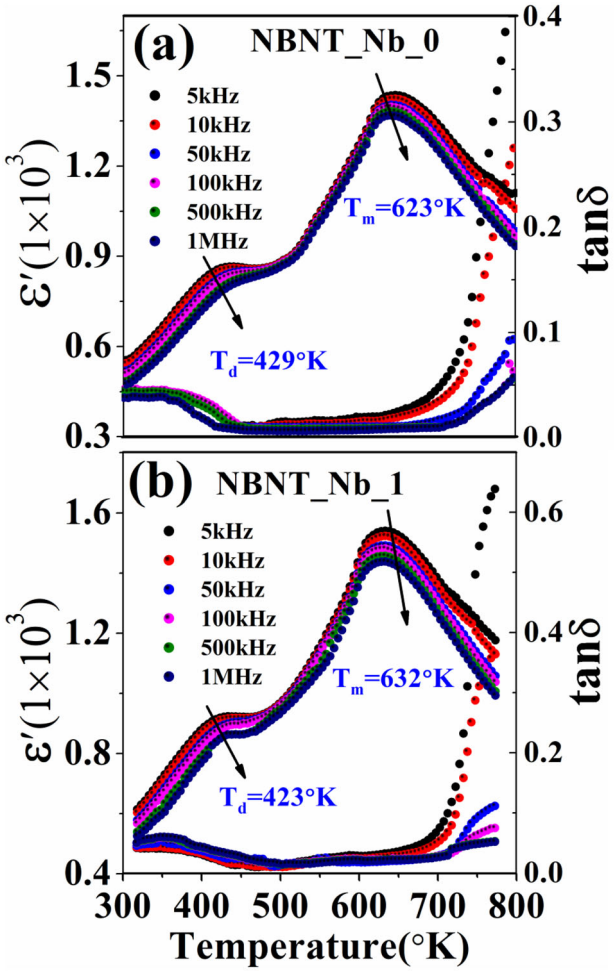

Figure 4. Temperature-dependent dielectric permittivity and loss of a) NBNT-Nb-0 and b) NBNT-Nb-1 ceramics in temperature intervals 30–450 °C at selective frequencies of (5, 10, 50, 100, 500 and 1000) kHz.

represents ferroelectric transition, is independent of applied field in NBNT ceramics.

In contrast, Nb^{5+} substituted NBNT-Nb-1 ceramics showed saturated *P*–*E* loops with reduced $E_c = 33\,kV\,cm^{-1}$ values at 313 K. On increasing temperature, the E_c and P_r values reduced progressively as shown in Figure 5c. Even at higher temperatures above 360 K, a duel shape pinched P-E hysteresis loop was observed. This represented that the FE order was likely to disappear above 360 K and an AFE order tends to appear. Therefore, the incorporation of Nb^{5+} in NBNT triggers monoclinic ferroelectric phase to AFE (tetragonal) state. The observation of AFE character is quite often in NBT based ceramics near to morphotropic phase boundary. Such AFE based materials exhibit giant electrocaloric effect rather than ferroelectric materials similar to $PbZrO_3$ based materials. In **Figure 6**c,d represents the variation of polarization as a function of temperature at five selected applied electric fields (10-10-50) $kV\,cm^{-1}$ for NBNT-Nb-1 and NBNT-Nb-1 ceramics, respectively. At low applied electric field, the polarization values decrease with temperature. Whereas at high field $\geq 40\,kV\,cm^{-1}$, the polarization is independent of temperature which represents ferroelectric transition is shifted towards high temperature with increasing field.[38]

The strain versus electric field (*S*–*E*) loops for NBNT-Nb-0 ceramics show a butterfly shape with an asymmetric feature due to the existence of an internal bias field. The observed maximum strain (S_{max}) = 0.12%, both in magnitude (positive and negative) and independent of observed temperature range indicate a typical ferroelectric character in the probed temperature range for NBNT-Nb-0 ceramics. In case of NBNT-Nb-1 ceramics, the gradual decreasing and eventually vanishes the negative strain region were observed with increasing temperature. Furthermore, a sudden increase of positive strain near about (S_{max}) = 0.25% over the electric field $80\,kV\,cm^{-1}$ reflects the inducing of relaxor behavior from the ferroelectric character. The measured values from the strain have been well coordinated with polarization loops representing ferroelectric to antiferroelectric for Nd^{5+} substituted in NBNT ceramics. Thus, these Nb^{5+} substituted NBNT triggered the antiferroelectric character, which can be useful for future applications in energy storage device.[30]

In various reports suggests, the electrocaloric (adiabatic) change in temperature (ΔT) and isothermal change in entropy (ΔS) is not only measured directly but also calculated indirectly with the help of temperature dependence of P-E loops, which is extracted by using Maxwell's relation.[39]

$$\Delta T = -\frac{1}{\rho C_p}\int_{E_1}^{E_2} T\frac{dp}{dT}dE \quad (1)$$

$$\Delta S = -\frac{1}{\rho}\int_{E_1}^{E_2} \frac{dp}{dT}dE \quad (2)$$

Here, *P* represents the polarization, *T* is the measured temperature, E_1 and E_2 are starting and final applied electric fields and C_p is specific heat, that is, $0.540\,J\,g^{-1}\,K^{-1}$ for NBNT-Nb-0, and $0.532\,J\,g^{-1}\,K^{-1}$ for NBNT-Nb-1 ceramics, respectively at RT were adopted from the literature.[40] Here ρ is the density of the ceramics is noted $5.9\,g\,cm^{-3}$ for NBNT-Nb-0 and $5.82\,g\,cm^{-3}$ for NBNT-Nb-1with the help of Archimedes method, respectively. The observed values are found to be very close to the pure NBT based ceramics.[41] The electrocaloric temperature variation (ΔT) as a function of temperature for both ceramics, obtained with varies in electric fields as shown in Figure 6a,b. Significant ECE values are obtained at high field for both ceramics in the vicinity ferroelectric to antiferroelectric transition region only. The maximum ECE temperature (ΔT) values at $50\,kV\,cm^{-1}$ are 0.69 K for NBNT-Nb-0 and 0.81 K for NBNT-Nb-1 ceramics, respectively. The observed values for both ceramics are found to be slightly higher than in many other recent reported NBT based ceramics and also comparable with lead based ceramics.[42] To make it further clear, we provided the bar chat with the comparative study between the available literatures on bulk ceramics and presented the reported values as seen in **Figure 7**.

© 2019 WILEY-VCH Verlag GmbH & Co. KGaA, Weinheim

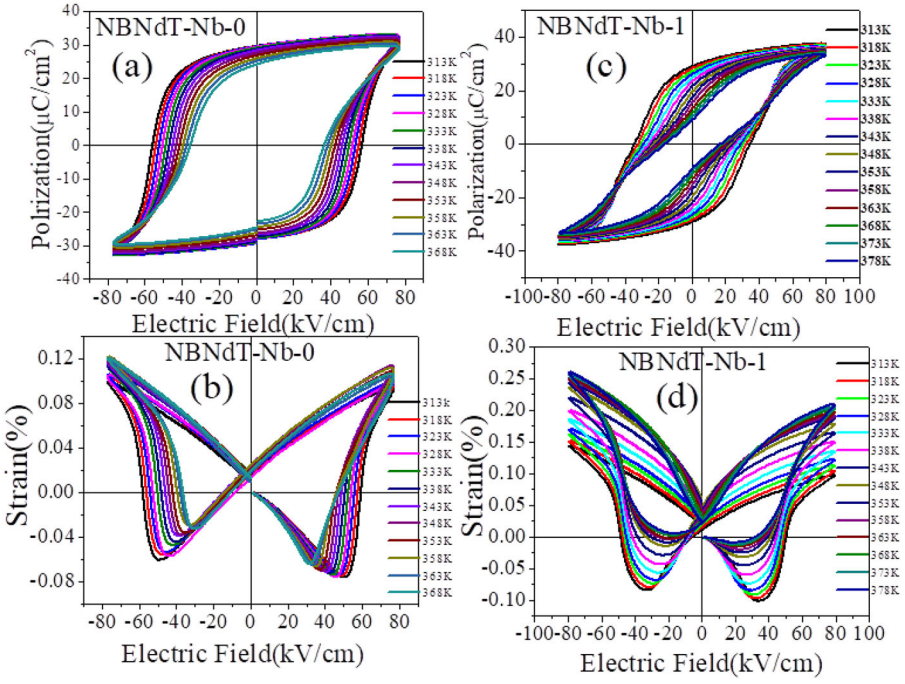

Figure 5. Temperature-dependent *P–E* loops of (a) NBNT-Nb-0 and (c) NBNT-Nb-1 ceramics. Temperature dependent *S–E* loops of (b) NBNT-Nb-0 and (d) NBNT-Nb-1 ceramics.

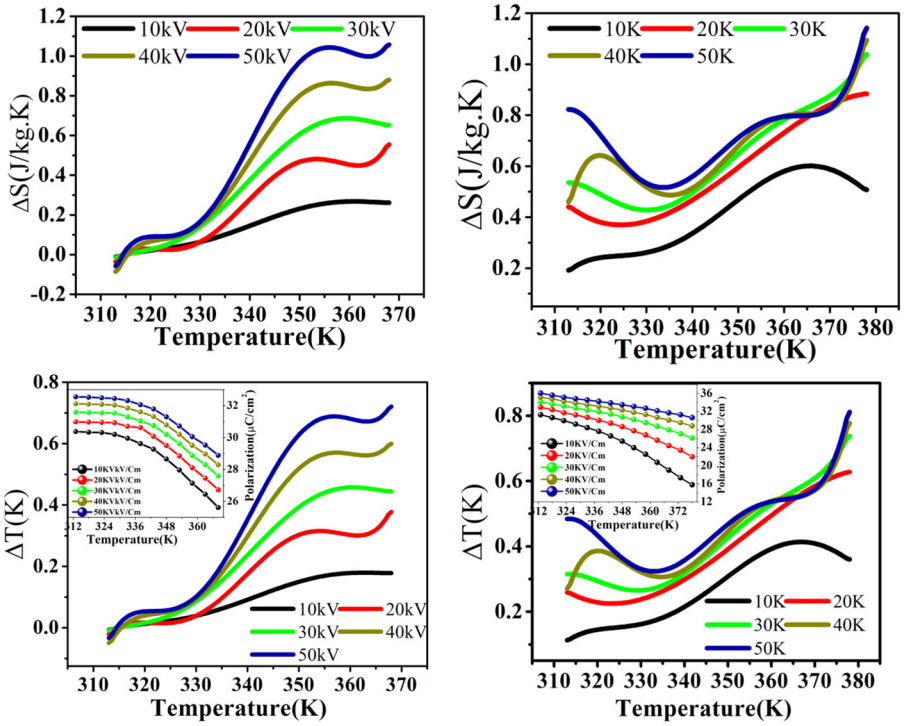

Figure 6. a,b) Electrocaloric (adiabatic) change in temperature (Δ*T*) as a function of temperature measured at (10-10-50) kV cm^{-1} electric fields for (a) NBNT-Nb-0 and (b) NBNT-Nb-1 ceramics. c,d) Entropy change (Δ*S*) as function of temperatures for (c) NBNT-Nb-0 and (d) NBNT-Nb-1 ceramics with different fields.

© 2019 WILEY-VCH Verlag GmbH & Co. KGaA, Weinheim

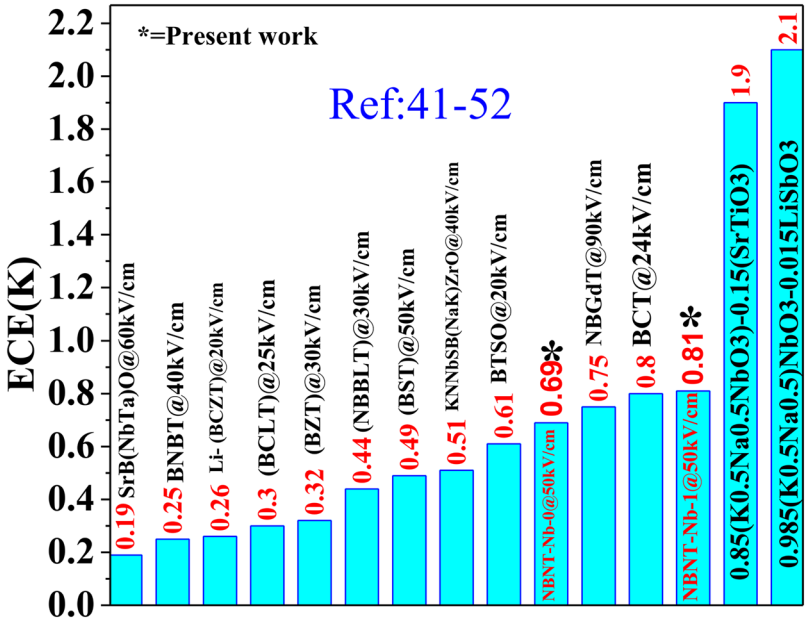

Figure 7. Comparative bar chart provided on recent reported ECE values of NBT based bulk ceramics from existing literature.

It is interesting to observe, both the ceramics are associated to two maxima points; the first one centered at around 310 K for NBNT-Nb-0 and 320 K for NBNT-Nb-1 ceramics, respectively. The second maxima shifted progressively to higher temperatures with increasing electric field for both ceramics. The isothermal entropy change (ΔS) showed a similar trend as the electrocaloric temperature change (ΔT) in both ceramics as observed in Figure 6c,d. The maximum isothermal entropy changes (ΔS) are 0.95 $Jkg^{-1}K^{-1}$ for NBNT-Nb-0 and 1.02 $Jkg^{-1}K^{-1}$ for NBNT-Nb-1 ceramics under the applied 50 $kV\,cm^{-1}$ at 360 K temperature. In addition, we have calculated the electrocaloric responsivity coefficient ($\Delta T/\Delta E$) for evaluating the performance of both specimens. The coefficient was found to be maximum at the electric field of 50 $kV\,cm^{-1}$ for NBNT-Nb-0 and NBNT-Nb-1 as shown in **Figure 8**, which is good agreement with the reported maximum ΔT (0.65 K) and ΔT (0.81 K) for NBNT-Nb-0 and NBNT-Nb-1 ceramics. The simultaneous enhancements in large ECE value are very much significant and reliable for application in the field of refrigeration technology.

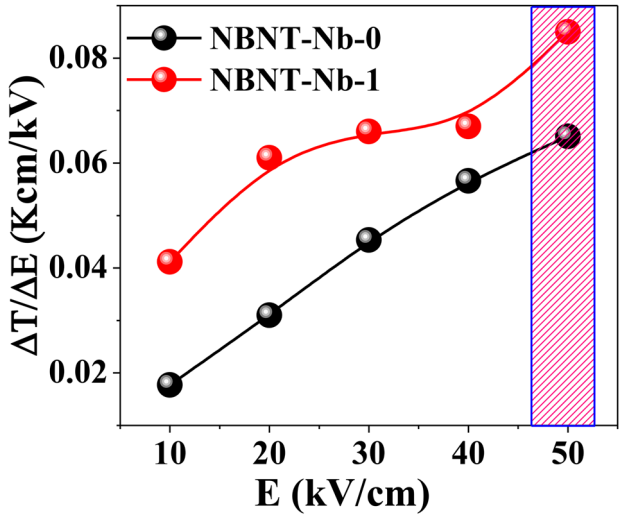

Figure 8. Variation of electrocaloric responsivity coefficients ($\Delta T/\Delta E$) with electric field for evaluating the performance of this specimen.

4. Conclusion

The XRD pattern of Nd^{3+} and Nb^{5+} co-substituted $(Na_{0.5}Bi_{0.49}Nd_{0.01})Ti_{1-x}Nb_xO_3$ revealed a structural single phase for NBNT-Nb-0 and coexistence of duel phases ($Cc+P4mm$) for NBNT-Nb-1 ceramics, respectively. This was further; confirmed with the help of the I–E characteristics. In dielectric studies shifting of T_m toward high temperature was observed and it was explained by using bond enthalpy concept. We also reported a large value in electrocaloric effect (ECE) and isothermal change entropy (ΔS) in both the ceramics with the help T-dependent P–E loops. The induce temperature ΔT and isothermal entropy change (ΔS) values were obtained at electric field 50 $kV\,cm^{-1}$ about 0.69 K, 0.95 $Jkg^{-1}K^{-1}$ for NBNT-Nb-0 and 0.81 K, 1.02 $Jkg^{-1}K^{-1}$ for NBNT-Nb-1 ceramics respectively. The noted value near at phase transition was found to be the same order as observed by other lead free ferroelectric materials. Hence, it can be conclude that $(Na_{0.5}Bi_{0.49}Nd_{0.01})Ti_{1-x}Nb_xO_3$ systems are expected to be a new promising candidate for lead-free dielectric and electrocaloric material in a great potential application in the field of refrigeration technology.

Acknowledgement

The Author S.A. gratefully acknowledges the financial support by Department of Science and Technology (DST), India to carry out this work, under the project EMR/2014/000761.

Conflict of Interest

The authors declare no conflict of interest.

Keywords

dielectrics and polarization, electrocaloric effect, lead-free piezoelectrics, X-ray diffraction

Received: January 2, 2019
Revised: February 24, 2019
Published online:

© 2019 WILEY-VCH Verlag GmbH & Co. KGaA, Weinheim

[1] Z .Kutnjak, J. Petzelt, R. Blinc, *Nature*. **2006**, *441*, 956.
[2] H .Takao, T. Tani, T. Nonoyama, K. Takatori, T. Homma, *Nature*. **2004**, *432*, 84.
[3] J .Peräntie, T. Correia, J. Hagberg, A. Uusimäki, *Electrocaloric Materials*, Springer, Berlin Heidelberg pp. 47.
[4] C .Long, H. Fan, P. Ren, *Inorg. Chem*. **2013**, *52*, 5045.
[5] G. Dong, H. Fan, M. Li, *J. Am. Ceram. Soc*. **2015**, *98*, 1150.
[6] X .Moya, S. Kar-Narayan, N. D. Mathur, *Nat. Mat*. **2014**, *13*, 439.
[7] S. M. Ke, H. T. Huang, H. Q. Fan, H. K. Lee, L. M. Zhou, *Appl. Phys. Lett*. **2012**, *101*, 082901.
[8] P. D. Thacher, *J. Appl. Phys*. **1968**, *39*, 1996.
[9] S. G. Lu, B. Rozic, Q. M. Zhang, Z. Kutnjak, X. Li, *Appl. Phys. Lett*. **2010**, *97*, 162904.
[10] A. S. Mischenko, Q. Zhang, J. F. Scott, R. W. Whatmore, *Science*. **2006**, *311*, 1270.
[11] T. Durga Rao, K. Raja Kandula, S. Asthana, *J. Appl.Phys*. **2018**, *123*, 244104.
[12] W. Geng, Y. Liu, X. Meng, L. Bellaiche, J. F. Scott, *Adv. Mater*. **2013**, *27*, 3165.
[13] G. Singh, I. Bhaumik, S. Ganesamoorthy, *Appl. Phys. Lett*. **2013**, *102*, 082902.
[14] X. Wang, F. Tian, C. Zhao, J. Wu, Y. Liu, B. Dkhil, *Appl. Phys. Lett*. **2015**, *107*, 252905.
[15] G. H. Haertling, *J. Ame. Ceram. Soc*. **1999**, *82*, 797.
[16] V. A. Isupov, *Ferroelectrics*. **1989**, *90*, 113.
[17] C. S. Tu, I. G. Siny, V. H. Schmidt, *Phys. Rev. B*. **1994**, *49*, 11550.
[18] G. Trolliard, V. Dorcet, *Chem. Mater*. **2008**, *20*, 5074.
[19] J. Y. Yi, J. K. Lee, *J. Phys. D: Appl. Phys*. **2011**, *44*, 415302.
[20] K. R. Kandula, S. S. K. Raavi, S. Asthana, *RSC Adv*. **2018**, *8*, 15282.
[21] Q. Li, J. Wang, L. Ma, H. Fan, Z. Li, *Bull. Mater. Sci*. **2016**, *74*, 57.
[22] W. P. Cao, W. L. Li, D. Xu, Y. F. Hou, W. D. Fei, *Ceram. Inter*. **2014**, *40*, 9273.
[23] M. Zannen, A. Lahmar, B. Asbani, *Appl. Phys. Lett*. **2015**, *107*, 032905.
[24] M. Zannen, A. Lahmar, Z. Kutnjak, J. Belhadi, *Solid State Sci*. **2017**, *66*, 31.
[25] K. R. Kandula, S. Asthana, S. S. K. Raavi, *Phys. Status Solidi A*. **2018**, 700915.
[26] M. K. Niranjan, T. Karthik, S. Asthana, *J. Appl. Phys*. **2013**, *113*, 194106.
[27] V. Dorcet, G. Trolliard, P. Boullay, *Chem. Matter*. **2008**, *20*, 5061.
[28] X. Wang, H. L. W. Chan, C. Choy, *Solid State. Commun*. **2003**, *125*, 395.
[29] F. Li, Y. Liu, Y. Lyu, Y. Qi, Z. Yu, C Lu, *Ceram. Inter*. **2017**, *43*, 106.
[30] K. R. Kandula, S. S. K. Raavi, S Asthana, *J. Alloy. Comp*. **2017**, *32*, 233.
[31] V. Pal, R. K. Dwivedi, O. P. Thakur, *Mater. Rese. Bullet*. **2014**, 51189.
[32] K. R. Kandula, S. S. K. Raavi, S. Asthana, *Ferroelectrics* **2017**, 5181300117.
[33] J. Wu, C. W. Nan, Y. Lin, Y. Deng, *Phys. Rev. Lett*. **2002**, *89*, 217601.
[34] A. S. Mischenko, Q. Zhang, J. F. Scott, R. W. Whatmore, *Science*. **2006**, *311*, 1270.
[35] A. S. Mischenko, Q .Zhang, R. W. Whatmore, *Appl. Phys. Lett*. **2006**, *89*, 242912.
[36] M. Zannen, A. Lahmar, B. Asbani, *Appl. Phys. Lett*. **2015**, *107*, 032905.
[37] D. Maurya, C. W. Ahn, S. Priya, *Adv. Electr. Ceram. Mater. II*, John Wiley & Sons, Inc, Hoboken (NJ) **2010**, pp. 47.
[38] Y. Bai, G. P. Zheng, S. Q. Shi, *Mater. Res. Bullet*. **2011**, *46*, 1866.
[39] A. K. Axelsson, F. Le Goupil, M. Valant, N. M. Alford, *Acta Mater*. **2017**, 124120-6.
[40] K. S. Srikanth, P. Satyanarayan, V. Rahul, *J. Austr. Ceram. Soc*. **2017**, *53.2*, 523.
[41] J. Shi, R. Zhu, X. Liu, B. Fang, N. Yuan, J. Ding, H. Luo, *Materials* **2017**, *10.9*, 1093.
[42] Y. Guo, H. Fan, C. Long, J. Shi, L. Yang, *J. Alloy. Comp*. **2014**, *610*, 189.
[43] J. Liu, W. Gong, Y. Yao, Q. Li, J. Jiang, Y. Wang, *J. Mater. Scien: Mater. Elect*. **2018**, *29.2*, 1075.
[44] F. Weyland, T. Eisele, S. Steiner, T. Frömling, *J. Europ. Ceram. Soc*. **2018**, *38.2*, 551.
[45] G. Chen, et al. *J. Alloy. Compd*. **2017**, *727*, 785.
[46] P. Z. Ge, X. G. Tang, Q. X. Liu, Y. P. Jiang, W. H. Li, *J. Mater. Sci. Mater. Electron*. **2017**, *29*, 1075.
[47] F. Weyland, T. Eisele, S. Steiner, *J. Eur. Ceram. Soc*. **2017**, 38551.
[48] J. Wang, X. Zhang, H. G. Piao, Z. Luo, C. Xiong, X. Wang, F. Yang, *Appl. Phys. Lett*. **2014**, 105102904.
[49] M Zannen, A Lahmar, Z Kutnjak, J Belhadi, *Solid State Sci*. **2017**, *66*, 31.
[50] K. S. Srikanth, R. Vaish, *J. Eur. Ceram. Soc*. **2017**, *37*, 3927.
[51] J. Koruza, B. Rožič, G. Cordoyiannis, Z. Kutnjak, *Appl. Phys. Lett*. **2015**, *106*, 202905.

© 2019 WILEY-VCH Verlag GmbH & Co. KGaA, Weinheim